Soaring styles of extinct giant birds and pterosaurs

Authors:

Yusuke Goto[1]*, Ken Yoda[2], Henri Weimerskirch[1], Katsufumi Sato[3]

Author Affiliation:

[1]*Centre d'Etudes Biologiques Chizé, CNRS – Université de la Rochelle, 79360 Villiers En Bois, France.*

[2]*Graduate School of Environmental Studies, Nagoya University, Furo, Chikusa, Nagoya, Japan.*

[2]*Atmosphere and Ocean Research Institute, The University of Tokyo, Chiba, Japan.*

Corresponding Author:

Yusuke Goto

Centre d'Etudes Biologiques Chizé, CNRS – Université de la Rochelle, 79360 Villiers En Bois, France.

e-mail: goto924@gmail.com

TEL: +814-7136-6220

Abstract

Extinct large volant birds and pterosaurs are thought to have used wind-dependent soaring flight, similar to modern large birds. There are two types of soaring: thermal soaring, used by condors and frigatebirds, which involves the use of updrafts to ascend and then glide horizontally; and dynamic soaring, used by albatrosses, which involves the use of differences in wind speed with height above the sea surface. However, it is controversial which soaring styles were used by extinct species. In this study, we used aerodynamic models to comprehensively quantify and compare the soaring performances and wind conditions required for soaring in two of the largest extinct bird species, *Pelagornis sandersi* and *Argentavis magnificens* (6–7 m wingspans), two pterosaur species, *Pteranodon* (6 m wingspan) and *Quetzalcoatlus* (10 m wingspans), and extant soaring birds. For dynamic soaring, we quantified how fast the animal could fly and how fast it could fly upwind. For thermal soaring, we quantified the animal's sinking speed circling in a thermal at a given radius and how far it could glide losing a given height. Consistently with previous studies, our results suggest that *Pteranodon* and *Argentavis* used thermal soaring. Conversely, the results suggest that *Quetzalcoatlus*, previously thought to have used thermal soaring, was less able to ascend in updrafts than extant birds, and *Pelagornis sandersi*, previously thought to have used dynamic soaring, actually used thermal soaring. Our results demonstrate the need for a comprehensive assessment of performance and required wind conditions when estimating soaring styles of extinct flying species.

Introduction

Flying animals have evolved a wide range of body sizes. Among them, there have been incredibly large species of birds and pterosaurs (Fig. 1). *Pelagornis sandersi* and *Argentavis magnificens* are the largest extinct volant birds. Their estimated wingspans reached 6–7 m (1–4), twice as large as that of the wandering albatross, the extant bird with the longest wingspan (Table 1). Several large species of pterosaurs appeared in the Cretaceous period. *Pteranodon,* presumably the most famous pterosaur, is estimated to have had a wingspan of 6 m (Table 1) (5). The azhdarchids are one of the most successful Cretaceous pterosaur groups and include many large species with wingspans of approximately 10 m (Table 1) (6–9). *Quetzalcoatlus northorpi*, one of the azhdarchid species, is regarded as one of the largest flying animals in history.

Discoveries of these giant winged animals have fascinated paleontologists and biologists for over a century. Their flight ability has been of great interest because their huge

size must significantly affect their flight. With increasing size, flapping becomes more costly; the power required to fly increases faster than the power muscles can produce. Two main arguments are often debated about the flight of extinct giants, both stemming from this physical constraint: the first is about whether they were able to take off (4, 10–12); the second is about what kind of soaring flight style they employed (1, 4, 13–15). This study focuses on the latter debate. Due to the high cost of flapping, large extant birds prefer to fly utilizing wind energy, that is, they prefer to soar. It is presumed that extinct large animals also employed soaring flight as their primary mode of transportation (1, 4, 14). For example, in *Quetzalcoatlus*, flapping flight might have required anaerobic exercises that were difficult to sustain for long periods of time (14).

There are two main soaring flight styles among extant birds: dynamic soaring and thermal soaring (16). In dynamic soaring, birds extract flight energy from wind shear—the vertical gradient in horizontal wind speed over the ocean (Fig. 2A). In extant birds, seabirds (e.g., albatrosses, shearwaters, and petrels) employ this soaring style and can routinely travel hundreds of kilometers per day over the sea. In thermal soaring, birds first fly circling in warm rising-air columns (thermals). They climb to a substantial height and then glide off in the desired direction while losing their height (Fig. 2C-E). By repeating this up-down process, birds travel over vast distances. Various terrestrial bird species (e.g., vultures, eagles, and storks) and seabirds (e.g., frigatebirds and pelicans) employ thermal soaring.

This study investigated which soaring styles were employed by four large extinct species, that is, *Pelagornis sandersi, Argentavis magnificens*, *Pteranodon*, and *Quetzalcoatlus*. Their soaring capabilities were quantified using two factors. The first is performance, for example, the available speed and efficiency of soaring. The second is the minimum wind speed required for sustainable soaring flight.

For thermal soaring, performance was evaluated in the gliding and soaring up phases. In the gliding phase, a bird's performance is its glide ratio, which is the ratio of distance a bird traverses to the height the bird loses to cover that distance, i.e., (glide ratio) = (horizontal speed)/(sinking speed) (Fig. 2E). A bird with a higher glide ratio can traverse a longer distance for the same amount of height lost as a bird with a lower glide ratio. Plotting a curve known as a 'glide polar' is the conventional method to quantify glide ratio and the associated speed in artificial gliders and birds (16). This curve is a plot of the sinking speed against horizontal speed when a bird glides in a straight line. We can determine the flyer's highest glide ratio and the associated travel speed by finding the line that passes the origin and tangents of the glide polar.

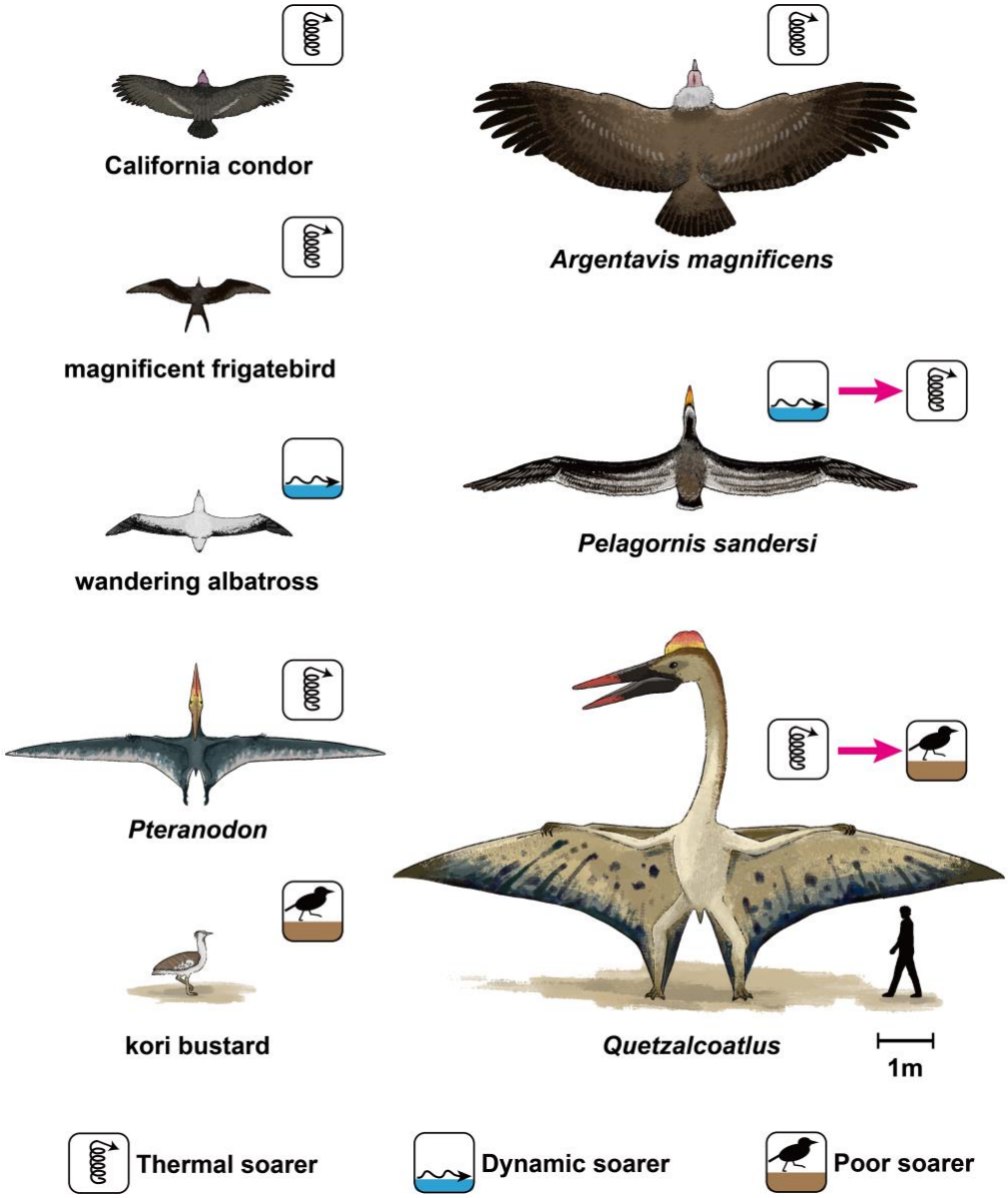

Fig. 1. A size comparison and soaring styles of extinct giant birds (*Pelagornis sandersi* and *Argentavis magnificens*), pterosaurs (*Pteranodon* and *Quetzalcoatlus*), the largest extant dynamic soaring bird (wandering albatross), the largest extant thermal soaring terrestrial bird (California condor), the largest extant thermal soaring seabird (magnificent frigatebird), and the heaviest extant volant bird (kori bustard). The icons indicate dynamic soarer, thermal soarer, and poor soarer and summarize the main results of this study. The red arrows indicate the transition from a previous expectation or hypothesis to the knowledge updated in this study.

	Species	Mass (kg)	Wingspan (m)	Wing area (m^2)	Aspect ratio	Wing loading	Ref
Extinct	*Pelagornis sandersi*	21.8, and 40.1	6.06, 6.13, 6.40 and 7.38	2.45 ~ 4.19	13.0, 14.0, and 15.0	51.0 ~ 161	(1)
	Argentavis magnificens	70.0	7.00	8.11	6.04	84.7	(4)
	Pteranodon	36.7	5.96	1.99	17.85	181	(5)
	Quetzalcoatlus	259	9.64	11.36	8.18	224	(5)
Dynamic soaring	wandering albatross (*Diomedea exulans*)	8.64	3.05	0.606	15.4	140	(48)*
	black-browed albatross (*Thalassarche melanophris*)	3.55	2.25	0.376	13.4	87.5	(49)*
	white-chinned petrel (*Procellaria aequinoctialis*)	1.37	1.4	0.169	11.6	79.5	(50)
Thermal soaring	magnificent frigatebird (*Fregata magnificens*)	1.52	2.29	0.408	12.8	36.5	(17)
	California condor (*Gymnogyps californianus*)	9.5	2.74	1.32	5.7	70.6	(4)
	brown pelican (*Pelecanus occidentalis*)	2.65	2.10	0.45	9.80	57.8	(17)
	black vulture (*Coragyps atratus*)	1.82	1.38	0.327	5.82	54.6	(17)
	white stork (*Ciconia ciconia*)	3.4	2.18	0.540	7.42	61.8	(4)
Non-Soaring	kori bustard (*Ardeotis kori*)	11.9	2.47	1.06	5.76	110	(16)

Table 1. Morphological values of examined species. *For the wandering albatross and the black-browed albatross, we used the averages calculated from the morphological values of males and females in the cited references (48, 49). For the kori bustard, we used the morphology data available in the *Flight* program (16).

The inverse of the line's slope and the speed at the tangent point correspond to the highest glide ratio and the associated horizontal speed, respectively. The performance in the soaring up phase is represented by the sinking speed during circling in a given radius. To achieve thermal soaring, a bird needs a higher upward wind speed than the circling bird's sinking speed (Fig. 2D). Because thermals have a stronger updraft in the center (Fig. 2C), the animal needs to

achieve not only low sinking speed but also a narrow turning radius to efficiently ascend through the thermal. A ‘circling envelope’ curve visualizes this performance and the required minimum updraft wind speed. This curve is a graph of the minimum sinking speed (i.e., the required minimum upward wind speed for ascent) against the radius of turn when a bird glides in a steady circle. Circling envelopes have been used to quantify the soaring up ability of extant bird species (16, 17).

For sustainable dynamic soaring, a certain amount of horizontal wind speed is essential. With respect to the performance of dynamic soaring, we used two metrics. For soaring animals, traveling fast enables them to save energy costs. Hence, the first dynamic soaring performance we measured was the maximum travel speed averaged over one dynamic soaring cycle under a given wind speed (Fig. 2B). In addition, the ability to travel in a desirable direction irrespective of unfavorable wind conditions is also necessary. In particular, traveling upwind is the most challenging situation for flying animals. Accordingly, the second performance we measured was the maximum value of the upwind speed, that is, the parallel component of the travel speed to the upwind direction averaged over one soaring cycle (Fig. 2B). We previously lacked an established framework to quantify the dynamic soaring performances and minimum required wind speed. In previous studies, the glide polar has been used to quantify the dynamic soaring ability of animals (1, 13). However, the glide polar assumes that birds glide in a straight line, which is not the case during the complicated process of dynamic soaring. Hence, the glide polar may be an insufficient metric to describe dynamic soaring performance. A numerical optimization method developed in the engineering field was recently proposed to quantify the dynamic soaring performance of birds, requiring wind conditions (18, 19). However, despite its effectiveness, the only animal to which this technique has been applied is the wandering albatross (18, 19); it has never been applied to extinct giant flyers.

The soaring performances and required wind conditions have not been evaluated comprehensively for the four giant extinct species summarized in Table 2. Table 2 shows three knowledge gaps. First, the wind condition and the performance of dynamic soaring have rarely been evaluated. This is due to the lack of a framework to assess dynamic soaring ability, as mentioned above. Second, the thermal soaring performance in the soaring up phase and the minimum required updraft wind speed have not been evaluated for *Pelagornis sandersi*, *Pteranodon*, and *Quetzalcoatlus*. Finally, recent studies estimated that the body masses of *Pteranodon* and *Quetzalcoatlus* were about three times heavier than previously expected (5, 10,20, 21), and the soaring abilities of these new heavy body masses have rarely been

evaluated.Based on these three gaps, we summarize the previous studies on these four species' soaring styles.

[*Pelagornis sandersi*] *Pelagornis sandersi* is predicted to be a dynamic soarer rather than a thermal soarer as its glide polar (and glide ratio that can be derived from its glide polar) is more similar to those of living dynamic soarers than those of living thermal soarers (1). However, this means our understanding of this species' soaring style has been based on just one metric, that is, its glide ratio (Table 2). Hence, evaluating other metrics of this species, i.e., the required wind conditions in dynamic and thermal soaring, and performance in dynamic soaring and in the soaring up phase of thermal soaring is important for a more accurate estimate of the soaring style of this species. A previous study cautiously calculated *Pelagornis sandersi*'s glide polars for 24 combinations of estimates (body mass = 21.8 and 40.1 kg, wingspan = 6.06, 6.13, 6.40, and 7.38, and aspect ratio = 13,14, and 15) to deal with morphological uncertainty. Hence, we also employed these estimates in this study.

[*Argentavis magnificens*] *Argentavis magnificens* is expected to be a thermal soarer. A previous study reported that the thermal soaring performance and required wind conditions of this species are comparable to living thermal soaring species based on glide polars and circling envelopes (4). This result is consistent with the fact that an *Argentavis* specimen was found on the foothills and pampas of Argentina, far from coastlines (4).

[*Pteranodon* and *Quetzalcoatlus*] Although assessments of the soaring abilities of *Pteranodon* and *Quetzalcoatlus* have been a long-standing issue, we still lack a comprehensive understanding of their soaring style due to many uncertainties in the estimates of their morphology, especially because of the significant changes in weight estimates around 2010. Previously, it was estimated that *Pteranodon* had a wingspan of around 7 m and a body mass of 16 kg, while *Quetzalcoatlus* had a wingspan of around 11 m and a body mass of 50–70 kg. Based on these estimates, previous studies argued that they were adapted to thermal soaring (22, 23) and others argued that they could also employ dynamic soaring (13). Around 2010, however, many studies with different approaches suggested that pterosaurs were much heavier than previously expected (5, 10, 20, 21). For example, Witton estimated that *Pteranodon* was 36 kg with a 5 m wingspan, and *Quetzalcoatlus* was 259 kg with a 10 m wingspan (5). Other studies also reported similar estimated values (10, 20, 21). Few studies have quantified the soaring performance of these species based on these new heavy body mass estimates. For example, Witton and Habib argued that *Pteranodon* was a dynamic soarer and *Quetzalcoatlus* was a thermal soarer by comparing the aspect ratios and the relative wing loadings of these

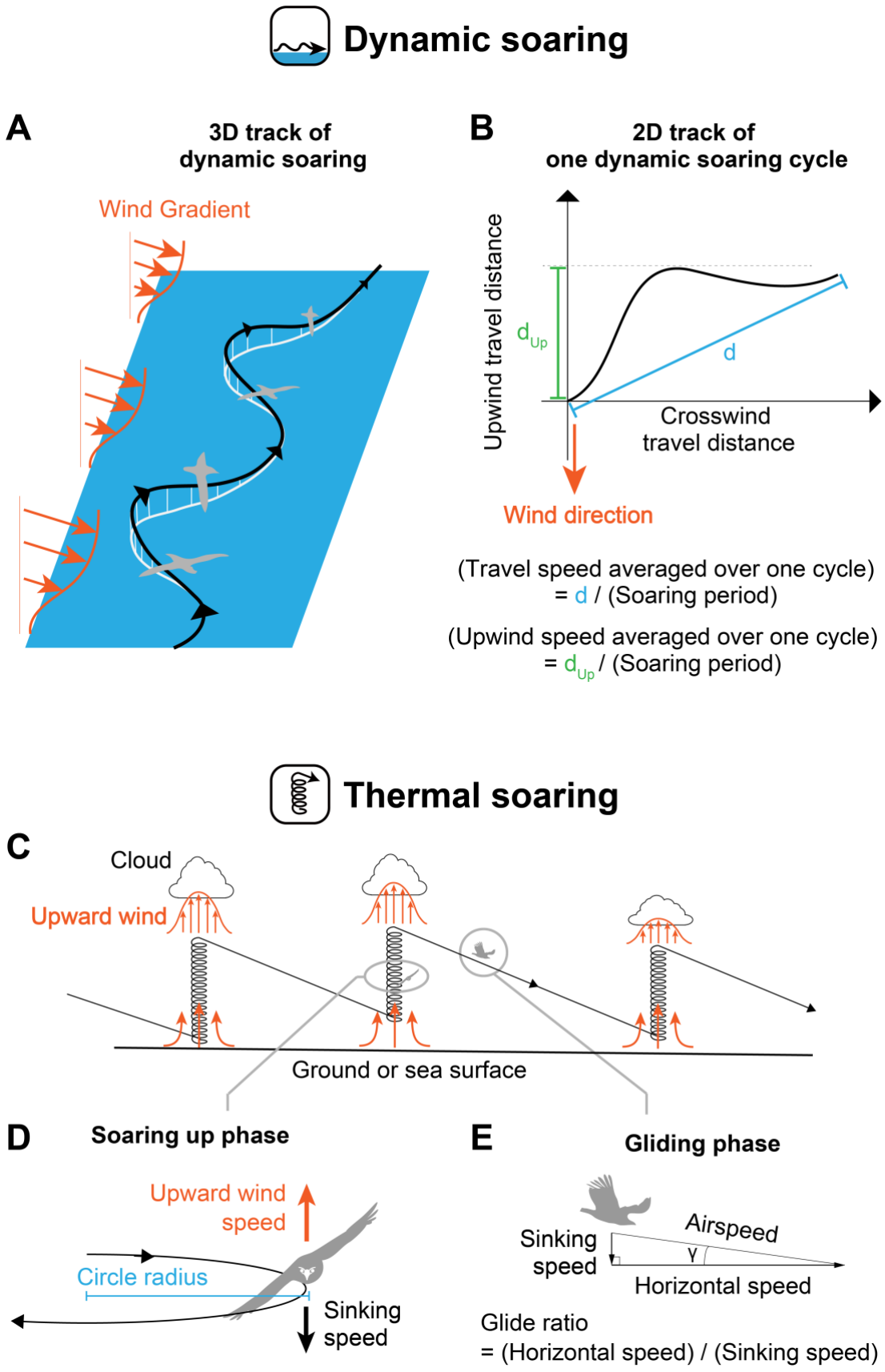
Dynamic soaring
A
3D track of
dynamic soaring
Wind Gradient
B
2D track of
one dynamic soaring cycle
Upwind travel distance
d_{Up}
d
Crosswind
travel distance
Wind direction
(Travel speed averaged over one cycle)
= d / (Soaring period)
(Upwind speed averaged over one cycle)
= d_{Up} / (Soaring period)
Thermal soaring
C
Cloud
Upward wind
Ground or sea surface
D
Soaring up phase
Upward wind
speed
Circle radius
Sinking
speed
E
Gliding phase
Sinking
speed
Airspeed
γ
Horizontal speed
Glide ratio
= (Horizontal speed) / (Sinking speed)

178

Fig. 2. Schematics of dynamic soaring and thermal soaring. (A) Example of a 3D track of dynamic soaring. Dynamic soaring species repeat an up and down process with a shallow S-shaped trajectory at the sea surface. By utilizing wind gradients, a species can fly without flapping. (B) Example of a 2D dynamic soaring trajectory of one soaring cycle. The travel speed averaged over one cycle is defined as the travel distance in one cycle (d) divided by the soaring period, and the upwind speed averaged over one cycle is defined as the upwind travel distance in one cycle (d_{Up}) divided by the soaring period. (C) Schematic of a thermal soaring cycle. (D) In the soaring up phase, a species soars in a steady circle. When there is upward wind that is greater than a species' sinking speed, the species can ascend in the thermal. The upward wind is stronger in the center of a thermal; therefore, achieving a small circle radius is advantageous for thermal soaring. (E) In the gliding phase a species glides in a straight line. The rate of horizontal speed to the sinking speed is equal to the rate of horizontal distance traveled to the height lost.

Species	Predicted Soaring Style	Dynamic soaring		Thermal soaring		
		Wind condition	Performance	Wind condition	Performance (Gliding)	Performance (Circling up)
Pelagornis sandersi	Dynamic soaring (1)		Glide polar (1)		Glide polar (1)	
Argentavis magnificens	Thermal soaring(4)			Circling envelope (4)	Glide polar (4)	Circling envelope (4)
Pteranodon (Body mass ≅ 35kg)	Thermal soaring (15) Dynamic soaring (14)* *based on aspect ratio and relative wing loading				Glide polar (15)	
Quetzalcoatlus (Body mass ≅ 250kg)	Thermal soaring (14)* *based on aspect ratio and relative wing loading					

Table 2. Previous studies that quantified the soaring performances and required wind conditions of *Pelagornis sandersi*, *Argentavis magnificens*, *Pteranodon*, and *Quetzalcoatlus* with recent heavy body mass estimates.

species with those of extant soaring bird species (5, 14). Conversely, a recent study quantified the cost of transport and sinking speed in the gliding of 128 pterosaur species and showed that azhdarchoid pterosaurs, including *Quetzalcoatlus*, had lower flight efficiency than the other

pterosaurs (24). However, despite these studies, we still have not been able to comprehensively quantify the performance and wind requirements of dynamic and thermal soaring of these species.

Furthermore, pterosaurs have a wing morphology that is completely different from that of birds and bats. Some studies reported that the wings of pterosaurs would have been associated with high-profile drag (drag stemming from the wings) (15, 25). Palmer experimentally measured profile drag in a wind tunnel experiment using reconstructed pterosaurs wings (15). With the experimentally derived profile drag, *Pteranodon*'s glide polars with the heavy body mass estimates were determined. Palmer concluded that *Pteranodon* adopted thermal soaring with a slow flight speed.

In this study, we aimed to address the knowledge gaps in the soaring abilities of these four extinct giants. First, we calculated the dynamic soaring performances and required wind speeds using a physical model and a numerical optimization method. This method has been developed in the engineering field and provides a framework to quantify dynamic soaring performances and required wind conditions. We applied this framework to the four giant extinct species and three extant dynamic soaring bird species with various sizes ranging from 1 to 9 kg [i.e., the wandering albatross (*Diomedea exulans*), the black-browed albatross (*Thalassarche melanophris*), and the white-chined petrel (*Procellaria aequinoctialis*)]. As the exact shape of the wind gradient is still poorly understood, we conducted the calculation under seven different wind conditions (Fig. 3A–C). In addition, we added an important modification to the previous models: the animal's wings do not touch the sea surface during their flight (Fig. 3D; and see Eq. 16 and its description in **Materials and Methods** for details). Second, we quantified the thermal soaring performances and the required upward wind speeds for the four extinct species, five extant thermal soaring species [the magnificent frigatebird (*Fregata magnificens*), the black vulture (*Coragyps atratus*), the brown pelican (*Pelecanus occidentalis*), the white stork (*Ciconia ciconia*), and the California condor (*Gymnogyps californianus*)], and kori bustard (*Ardeotis kori*), the heaviest extant volant bird that does not soar. These values were calculated using the established framework (i.e., glide polars and circling envelopes). Third, to quantify the soaring performances of *Pteranodon* and *Quetzalcoatlus*, we used the recent heavy body mass estimates (5). The profile drag coefficients of the pterosaurs (C_{Dpro}) were explored for two different cases: the same value as for birds (C_{Dpro} = 0.014) (16) and a higher value based on reconstructed pterosaur wings (C_{Dpro} = 0.075) (15, 25).

Results

Dynamic soaring

Our computation results indicate that *Argentavis magnificens* and *Quetzalcoatlus* could not have employed dynamic soaring (Fig. 4 A–C). Both species showed lower dynamic soaring performances and higher required wind speeds for dynamic soaring than the extant dynamic soaring species under all wind conditions tested in this study.

The dynamic soaring performances and required wind speeds of *Pelagornis sandersi* and *Pteranodon* varied substantially with the assumed morphology and shape of the wind gradient, especially the height where the steep wind speed change occurs (Fig. 4 A–C).

When *Pteranodon* was analyzed with a high-profile drag coefficient it showed poor performance and required strong winds compared with extant species, suggesting that

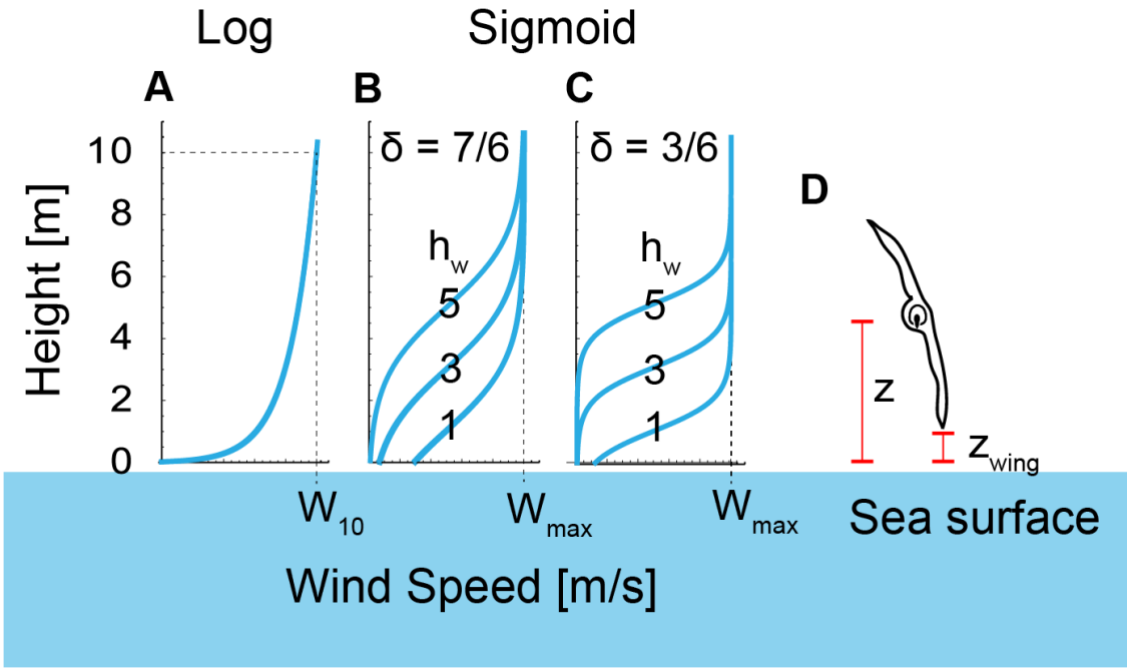

Fig. 3. (A-C) Wind shear models explored in this study. (A) Logarithmic wind gradient model. The wind speed at height 10 m was defined as W_{10}. (B) Sigmoidal wind shear model with a wind shear thickness of 7 m (δ = 7/6) and a shear height (h_w) of 1, 3, or 5 m. (C) Sigmoidal wind shear model with a wind shear thickness of 3 m (δ = 3/6) and a shear height of 1, 3, or 5 m. The maximum wind speed of the sigmoidal model is represented as W_{max}. (D) Schematic of a soaring bird. Its height from the sea surface is represented as z and the height of the wingtip is represented as z_{wing}. We constrained the models so that the wing tip did not touch the sea surface, i.e., $z_{wing} \geqq 0$.

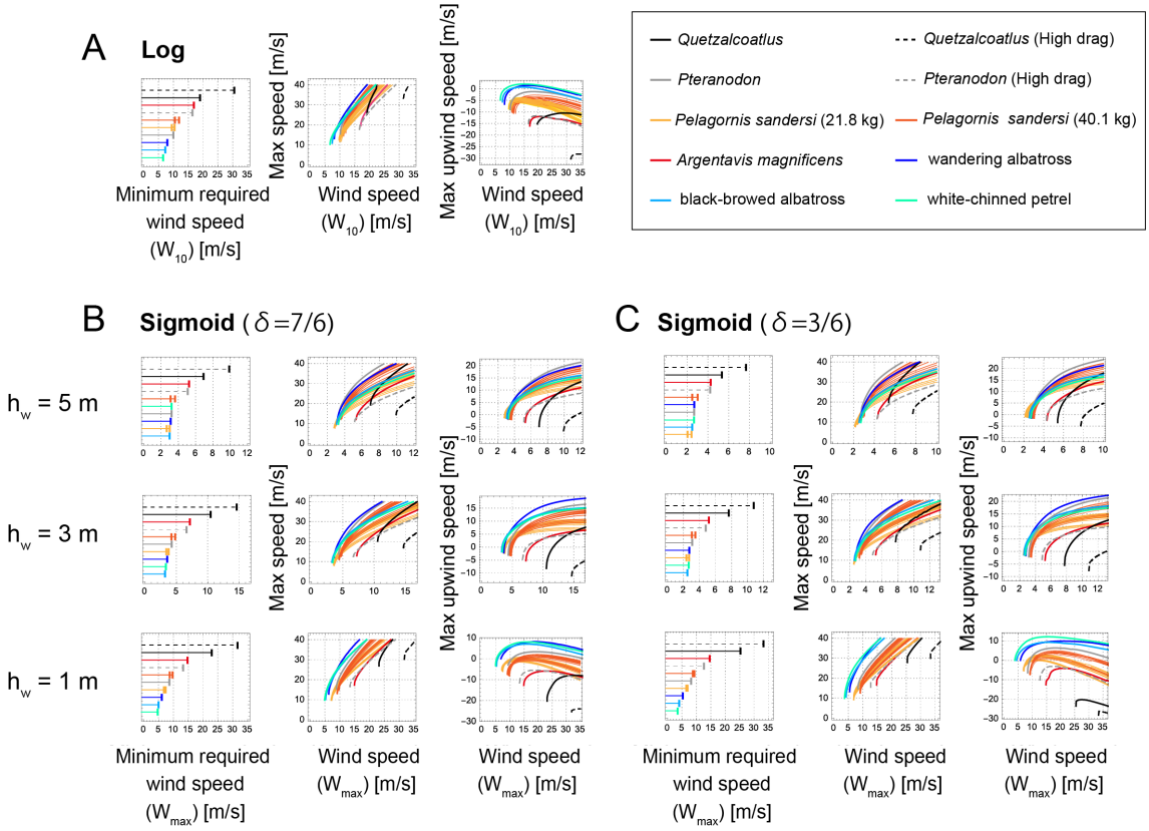

Fig. 4. Required minimum wind speeds and dynamic soaring performances of extinct and extant animals. (A) Results of the logarithmic wind model. (B) Results of the sigmoidal wind model with a wind shear thickness of 7 m (δ = 7/6) and wind shear height (h_w) of 1, 3, or 5 m. (C) Results of the Sigmoidal wind model with a wind shear thickness of 3 m (δ = 3/6) and a wind shear height (h_w) of 1, 3, or 5 m. The first column shows the minimum required wind speed for sustainable dynamic soaring. The second column shows the maximum travel speed averaged over one soaring cycle, in response to wind speed. The third column shows the maximum upwind speed averaged over one soaring cycle, in response to wind speed.

Pteranodon did not employ dynamic soaring. When *Pteranodon* was analyzed with a low-profile drag coefficient value, its performance outperformed that of extant birds when the wind change was located high from the sea surface (sigmoidal wind condition with h_w = 5 and 3). When the wind speed change was located close to the sea surface (logarithmic model and sigmoidal wind condition with h_w = 1), *Pteranodon* showed a poor flight performance and required a high wind speed. It required a stronger wind speed than the extant dynamic soaring species, except for in

sigmoidal wind conditions with h_w = 5. Hence, *Pteranodon* could not employ dynamic soaring when a high-profile drag was assumed. Conversely, when a low-profile drag was assumed, *Pteranodon* was capable of dynamic soaring but required strong wind conditions.

For *Pelagornis sandersi*, the results were highly dependent on body mass. With heavy body mass estimates (40.1 kg), *Pelagornis sandersi* required higher wind speeds than extant dynamic soaring species, irrespective of the wind conditions. The performance was superior to extant species for some morphology estimates when the shear height was high from the sea surface (sigmoidal wind condition with h_w = 5 and 3 m), but inferior when the wind speed change was located close to the sea surface (logarithmic model and sigmoidal wind condition with h_w = 1). When lower body mass estimates were used (21.8 kg), *Pelagornis sandersi* required lower wind speeds, but its performance (maximum speed and maximum upwind speed) was distinctively lower than that of extant species. Hence, *Pelagornis sandersi* required harsh wind conditions for dynamic soaring when a 40.1 kg body mass was assumed, and it was poor at dynamic soaring when a 21.8 kg body mass was assumed.

The performances of all species varied with the value of h_w, and the variation was especially distinct for large species in contrast to that of white-chinned petrels (Fig. 4 B and C). This variation was due to wingtip boundary conditions. Animals can attain more energy when passing through large wind speed gradients, but when large gradient changes are close to sea level, large animals are unable to use the wind speed gradient efficiently because their wings limit the altitude available to them. In other words, our results show that it is not enough to discuss the ability of dynamic soaring in terms of morphology and glide polars alone. Although the long, thin wings that reduce drag in extant dynamic soaring birds are suited for dynamic soaring (16, 26), detailed dynamic models have shown that excessively long wings can also inhibit efficient dynamic soaring.

Thermal soaring

Extinct species showed high gliding performances with maximum glide ratios ranging from 11 to 22 (Fig. 5A), which are comparative to those of extant species (from 11 to 18); nevertheless, *Quetzalcoatlus* had the lowest soaring efficiency (i.e., 8) among the other species when a high drag coefficient was assumed (C_{Dpro} = 0.075).

With respect to the soaring up phase, all of the extinct giant flyers, except for *Quetzalcoatlus*, had performances equivalent to or better than the extant species (Fig. 5B). As a previous study has already shown, the circling up performance of *Argentavis magnificens* was comparable to that of the California condor, one of the largest living thermal soarers (4). The

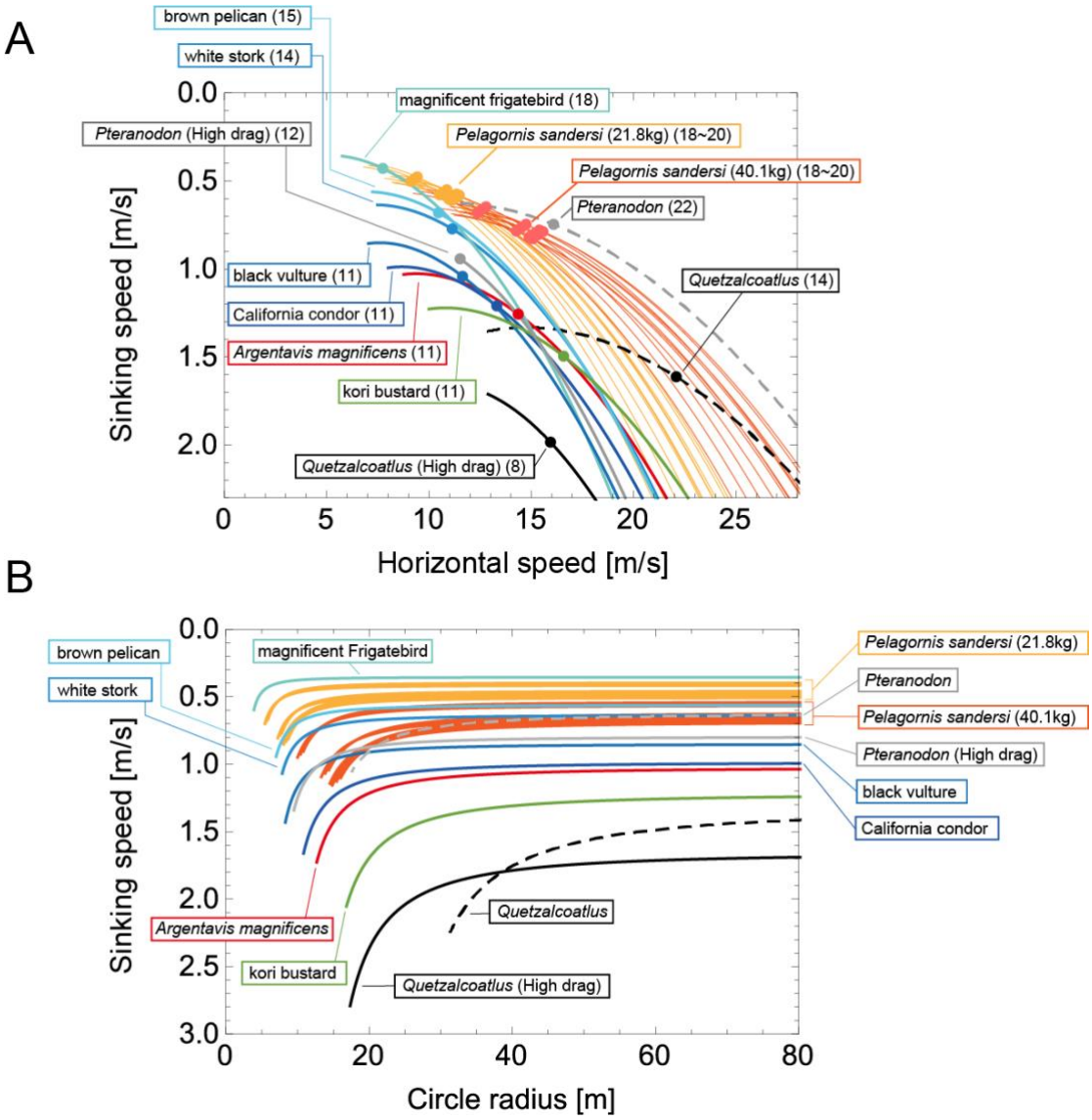

Fig. 5. (A) Glide polars and (B) circling envelopes of extinct species, extant thermal soaring species, and the kori bustard, the heaviest rarely flying bird. The solid line of *Pteranodon* and *Quetzalcoatlus* represents the result of a low-profile drag coefficient (CD_{pro} = 0.014), similar to bird species (16), and the dashed line represents the result of a high-profile drag coefficient (CD_{pro} = 0.075) based on the reconstruction of pterosaur wings (15, 25). In (A), the highest glide ratios of each species are shown on the right side of species names. Fig. B shows a circle envelope with a bank angle of up to 45°. The turning radius becomes smaller as the bank angle is increased.

performance of *Pteranodon* was comparable to that of living thermal soarers, irrespective of the value of the profile drag coefficient (C_{Dpro} = 0.014 or 0.075). With a higher

drag coefficient (C_{Dpro} = 0.075), a narrower circling radius was achieved by *Pteranodon*, and its circling envelope was very similar to that of the black vulture. The thermal soaring ability of *Pelagornis sandersi* when a light mass was assumed (21.9 kg) was outstanding. It outperformed many extant thermal soaring species in soaring up ability, and was even comparable to the magnificent frigatebirds, the champion of thermal soaring among extant species. Even with a heavier body mass estimate (40.1 kg), *Pelagornis sandersi* still outperformed or was comparable to many other species.

Among the four extinct giant animals investigated in this study, the soaring up performance of *Quetzalcoatlus* was exceptionally low. It required the strongest upward wind speed and the widest circle radius. Its performance was even lower than that of the kori bustard, one of the heaviest volant extant birds that spend most of their time on land and only fly in emergencies, such as when they are under predation risk.

Discussion

Using detailed physical models of soaring birds, we computed and compared the dynamic and thermal soaring performances and the required wind conditions for soaring of four extinct giant flyers with those of extant dynamic and thermal soaring species. Our results indicate that *Argentavis magnificens* and *Pteranodon* were thermal soarers, confirming previous studies (4, 15). However, our results also indicate that *Quetzalcoatlus* could not efficiently perform dynamic nor thermal soaring. In addition, although *Pelagornis sandersi* was considered a dynamic soaring species in a previous study (1), our results suggest that it was a thermal soaring bird. In the following, we discuss our results in detail for *Quetzalcoatlus* and *Pelagornis sandersi* and then describe future issues that need to be addressed for a better understanding of the soaring styles of extinct giant species.

Quetzalcoatlus

There has been a heated debate about the flight capability of *Quetzalcoatlus*. The focal issues have been whether or not *Quetzalcoatlus* could take off and if it was capable of sustained flapping flight. Researchers are divided between the opinion that it was too heavy to take off (10, 13, 27) and the opinion that it was able to take off by using quadrupedal launching, like some bats (11, 14). In addition, detailed observations of fossils are also presented as evidence that the giant azhdarchids, including *Quetzalcoatlus*, were capable of flight; for example, a huge deltopectoral crest on their humeri, which would have anchored muscles for flapping flight (28).

While there is some debate as to whether or not giant pterosaurs could have taken off, it has been widely accepted that if they were able to take off their primary mode of travel would have been thermal soaring rather than flapping flight. Witton and Habib applied a model of bird flap-gliding flight (16) to *Quetzalcoatlus*, and they found that this species' flapping flight required anaerobic movement and was difficult to sustain for long periods of time; therefore, it must have relied on wind energy for long-distance travel (14). They also concluded that *Quetzalcoatlus* used thermal soaring, based on a comparison of its morphology with that of birds (5, 14).

Our results revealed that *Quetzalcoatlus* had a poor ability to use thermals to ascend. It required a larger turning radius and stronger updraft than the terrestrial kori bustard, let alone species that use thermal soaring. Whether *Quetzalcoatlus*, with the soaring performance shown in Fig. 5, could routinely travel long distances by thermal soaring is beyond the scope of this study because of the need to examine in detail the wind conditions in their habitat at the time they lived. However, the results of this study alone suggest that *Quetzalcoatlus* performed poorly at thermal soaring compared with modern and other extinct species, and that the wind conditions under which thermal soaring was possible were limited. This poor thermal soaring performance was due to the large wing loading associated with the large body size. As shown in the *Materials and Method*s, the turning radius was proportional to the wing loading to the power of one half (eq. 19), and the descent speed during the turn was also proportional to the wing loading to the power of one half, if the effect of the organism's wing length adjustment was ignored (eqs. 18 and 20, and see also (26)). Since the wing loading is approximately proportional to body size, a giant *Quetzalcoatlus* required thermals with wider radius and stronger updraft for thermal soaring.

The wing loading also explains why the results of the present study are not consistent with the claims of previous studies that *Quetzalcoatlus* was adapted to thermal soaring (5, 14). Previous studies compared aspect ratios and relative wing loadings (wing loading divided by body size) between birds, bats, and pterosaurs and concluded that *Quetzalcoatlus* was adapted to thermal soaring because it was in the domain of thermal soaring birds (and, using the same procedure, it was concluded that *Pteranodon* was adapted to dynamic soaring). Interspecies comparisons of aspect ratios and relative wing loadings have been made for birds and bats for the purpose of examining the relationship between wing morphology and ecology (29, 30). However, caution should be taken in evaluating soaring ability with this size-independent variable (i.e., relative wing loading) because the thermal

soaring ability is inevitably size-dependent, as explained above. When evaluating soaring performance from animal morphology, performance and wind requirements calculated from morphology based on laws of physics (as conducted in this study and (24)) should be more desirable, as taking an inappropriate morphology as a variable may lead to erroneous results. For example, a fictional bird that is 10,000 times larger than but geometrically similar to frigatebirds (i.e., 230 km wingspan and 1.5×10^7 t body mass) needs, in theory, a turning radius and upward wind speed approximately 100 times larger than that of frigatebirds to conduct thermal soaring; however, the aforementioned size-independent metrics method outputs the unrealistic estimation that this bird was as efficient as frigatebirds in thermal soaring.

Recent anatomical studies of the azhdarchid pterosaurs have reported that their skeletal structure shows adaptations to terrestrial walking and suggested that they were terrestrial foragers (31, 32). Furthermore, recent phylogenetic analysis showed that the azhdarchoid pterosaurs differed from other pterosaurs in that they had evolved in the direction of increasing the cost of transport of flapping flight and the sinking speed of gliding (24). Taking into account the adaptations for walking (31, 32), the humeri feature indicating flapping flight capability (28) but not sustainable flapping flight (14), phylogenetic tendency of decreasing flight efficiency (24), and the low thermal soaring ability, we suggest that the flight styles of *Quetzalcoatlus* and other similar-sized azhdarchid species were similar to those of the bustard or hornbill that spent most of their time on land and rarely flew, except in critical emergencies. Alternatively, they may have routinely flown in early stages of their life history, but as they matured, wing loading would increase, and they would spend most of their time on land.

Pelagornis sandersi

Previously, it was reported that *Pelagornis sandersi* was a dynamic soarer like the albatross, rather than a thermal soarer like frigatebirds (1). However, we argue that this species is highly adapted for thermal soaring rather than dynamic soaring. The conclusion of the previous study was based on the glide polars of *Pelagornis sandersi*, which were more similar to those of the wandering albatrosses than those of frigatebirds; glide performance was the only criterion used to evaluate its soaring style. In this study, we quantified other performances and the required wind conditions, which enabled us to evaluate the soaring style of *Pelagornis sandersi* from multiple perspectives.

Our results indicated that the dynamic soaring performance of *Pelagornis sandersi* was generally inferior to that of extant dynamic soaring species, although there were substantial

variations depending on wind conditions and morphology estimates. One of the factors contributing to the poor dynamic soaring ability of this species was an inability to efficiently exploit the wind speed gradient due to long wings limiting the height above sea level at which the bird could fly. Note that this effect could not be assessed by the glide polars.

Conversely, the thermal soaring ability of *Pelagornis sandersi* was outstanding regardless of the morphology estimates used. It could circle in narrow thermals with a low sinking speed, as in extant species. Its performance to soar up thermals was even comparative to that of the frigatebird, the champion of extant thermal soaring species. In addition, its glide ratio was also high, outperforming most of the extant thermal soaring species. Accordingly, *Pelagornis sandersi* showed high performances both in the ascent and gliding phase of thermal soaring, indicating that this species was highly adapted to thermal soaring. Considering that *Pelagornis sandersi* was found close to the coast, this result indicates that *Pelagornis sandersi* was well adapted to capture a weak updraft above the sea and could stay aloft for a long time with limited flapping and traveled long distances like frigatebirds.

<u>Future issues</u>

In this section, we discuss some of the simplifications used in this study and issues that we believe need to be examined in the future. The first issue is flight stability. In this study, a steady wind environment was assumed, but actual wind environments fluctuate. In such a fluctuating real-world environment, stability is an important factor that determines the success or failure of flight (33, 34). To simplify our calculations, we did not address stability, but it is important to examine the flight stability of these extinct and extant birds using more detailed morphological information in the future.

The next issue is that the actual wind environment experienced by animals is still largely unknown. For dynamic soaring, the specific form of the wind speed gradient experienced by birds is unknown—for example, whether there is a logarithmic or sigmoidal gust in the shadows of the waves—and information on the height and thickness of the wind speed gradient is not yet known. For this reason, we evaluated performance under various wind conditions (Fig. 3). For thermal soaring, it is also unknown how much updraft animals experience at a given turning radius or the distance between thermals. Recent advances in tracking technology have made it possible to record details of the motion of birds in dynamic and thermal soaring (35–39). We believe that these data will provide information that will help us to understand our results and improve our model, such as the real wind environment experienced by animals (39–43). In

addition, it is also important to consider the paleoenvironmental aspects of the wind environment at the time of the extinct species' inhabitation. For example, we have shown that *Quetzalcoatlus* had a lower thermal soaring capacity than the extinct species. Paleoclimatic estimates may help us to understand whether the species had a favorable wind environment that allowed it to use thermal soaring as its primary mode of transport, even with their poor soaring up ability.

Finally, we would like to emphasize the importance of a comprehensive assessment of soaring performance and wind requirements of each soaring style, as we have done in this study. Although a great deal of previous research has been done on the soaring performance of extinct species, there have been several evaluation gaps. Our approach filled these gaps and allowed us to examine the soaring style of extinct giants from multiple perspectives, reaching different conclusions about the soaring styles of *Quetzalcoatlus* and *Pelagornis sandersi*. Future analyses that take into account the above issues will be necessary to more accurately estimate the soaring ability of extinct giants and thus their paleoecology, which may lead to different conclusions than those of this study. However, the importance of the framework presented here for a comprehensive assessment of soaring flight performance and wind requirements remains unchanged. We hope that this study will serve as a springboard for future discussions of soaring capabilities of extinct species.

Materials and Methods

The dynamics of soaring animals are described using the equations of motion (EOM). We first describe the EOM and parameters therein. Using the EOM, we can calculate soaring performances and the wind speeds required for sustainable soaring. We then describe the calculation procedure for dynamic soaring and thermal soaring, respectively.

<u>Aerodynamic forces and parameters</u>

We regard an animal as a point of mass. The dynamics of the animal's three-dimensional position $\boldsymbol{X}(t)$ and velocity $\boldsymbol{V}(t)$ are represented by the following EOMs:

$$m\frac{d\boldsymbol{V}(t)}{dt} = \boldsymbol{L} + \boldsymbol{D} + m\boldsymbol{g} \qquad [1]$$

$$m\frac{d\boldsymbol{X}(t)}{dt} = \boldsymbol{V}(t) \qquad [2].$$

When an animal is soaring, three forces—gravitation (*m***g**), lift force (***L***), and drag force (***D***)—act on it. Gravitation *m**g*** is a product of the constant of gravitation (***g***) and mass of the bird (*m* kg), and its direction is towards the ground. The direction of the lift force ***L*** is dorsal and perpendicular to the air velocity. Drag force ***D*** is against the air velocity. For the analysis of dynamic soaring, we assumed that wind blow is along the y-axis and represent these EOMs in a different way by transforming the ground velocity to pitch γ, yaw ψ, bank angle ϕ, and airspeed *V* using the following equations (19):

$$m\frac{dV}{dt} = -D - mg\sin\gamma + m\frac{\partial W(z)}{\partial z}\frac{dz}{dt}\cos\gamma\sin\psi \qquad [3],$$

$$mV\frac{d\gamma}{dt} = L\cos\phi - mg\cos\gamma - m\frac{\partial W(z)}{\partial z}\frac{dz}{dt}\sin\gamma\sin\psi \qquad [4],$$

$$mV\cos\gamma\frac{d\psi}{dt} = L\sin\phi + m\frac{\partial W(z)}{\partial z}\frac{dz}{dt}\cos\psi \qquad [5],$$

$$\frac{dx}{dt} = V\cos\gamma\cos\psi \qquad [6],$$

$$\frac{dy}{dt} = V\cos\gamma\sin\psi - W(z) \qquad [7],$$

and

$$\frac{dz}{dt} = V\sin\gamma \qquad [8],$$

where *W*(*z*) represents the wind gradient. A specific form is given in the latter subsection. *L* represents the strength of the lift force, and *D* represents that of the drag force. The aerodynamic theory asserts that these values are

$$L = |\boldsymbol{L}| = \tfrac{1}{2}\rho C_L S_{\mathrm{W}} V^2 \qquad [9]$$

and

$$D = |\boldsymbol{D}| = \frac{1}{2}\rho C_{\mathrm{Dpro}} S_{\mathrm{W}} V^2 + \frac{1}{2}\rho C_{\mathrm{Dpar}} S_{\mathrm{B}} V^2 + \frac{\rho(kC_{\mathrm{L}}^2)}{2\pi R_a} S_{\mathrm{W}} V^2 \qquad [10].$$

Here, ρ is air density and was set to ρ = 1.225 kg m^{-3} as in a previous study (1). This is the International Standard Atmosphere values for sea level and 15°C. C_L represents the lift coefficient. S_W represents the wing area. The drag is composed of three terms. The first term is the profile drag that stems from friction on the body. C_{Dpro} is the profile drag coefficient. For birds, a C_{Dpro} of 0.014 was employed following previous studies (1, 16). However, based on the reconstruction of pterosaur wings and a wind tunnel experiment, some studies have argued that the pterosaur profile drag coefficient is much higher (approximately 0.05–0.1) (15, 25). Hence, for the profile drag of *Pteranodon* and *Quetzalcoatlus*, we explored two cases: a bird-like low-profile drag of 0.014 and an experimentally based high-profile drag of 0.075 (we note that, although the experiments in the previous study assumed a pterosaur with a wing span of approximately 6 m (15), we assumed that the result would not vary significantly with the size of *Quetzalcoatlus*). The second term is the parasite drag stemming from friction on the wing, where the C_{Dpar} is the parasite drag coefficient, and S_B is the body frontal area. We used the following recently recommended formula

$$C_{\mathrm{Dpar}} S_{\mathrm{B}} = 0.01 S_{\mathrm{W}} \qquad [11]$$

on the practical basis that neither C_{Dpar} nor S_B is exactly known (26). The third term is the induced drag that stems from the lift force. R_a represents the aspect ratio ($R_a = b^2 / S_W$, where b is the wingspan). k is the induced drag factor; we set k to 1.1, as in previous studies (1, 14, 16). The lift coefficient has a maximum value; for birds, we set C_L to $\leq$ 1.8 (16). As the aerodynamic properties of pterosaurs can differ from those of birds, and the wind tunnel experiment indicated that C_L reached more than 2.0 (15), we set the pterosaurs' lift coefficient to $\leq$ 2.2, the same value used in a previous study on pterosaur gliding ability (14).

The remaining parameters in the EOMs are body mass (m), wingspan (b), and wing area (S_w). For these morphological parameters of extant birds, we used values reported in previous studies. For *Pelagornis sandersi*, we used 24 combinations of estimates proposed in a previous study (1). For *Argentavis magnificens*, we used the estimates in (4). For *Pteranodon* and *Quetzalcoatlus*, we used the recent estimates for heavy pterosaurs, as reported in (5). These values are shown in Table 1.

The EOMs include variables that soaring animals can control, that is, bank angle ϕ(t) and lift coefficient C_L. Although these variables are time-dependent, for simplicity, we assumed that the animals keep their lift coefficients at a constant value. Hence, using a time

series for bank angle, a constant value of C_L, and values of parameters, the dynamics of the soaring animals were determined with EOM.

Quantification of the dynamic soaring performance and the required minimum wind speed

Wind gradient model

We explored two types of wind gradients. The first was the logarithmic model represented as

[Logarithmic wind gradient model]

$$W_{\mathrm{Log}}(z) = W_{10} \log\left[\frac{z/h_{\min}}{10/h_{\min}}\right] \quad [12].$$

This function is defined at $z > h_{\min}$. We set $h_{\min}$ to 0.03 [m], following a previous study (18). W_{10} is the wind speed at height z = 10 m. This model is deemed to be a good model of the average wind field in the first 20 m above the sea surface, assuming a flat sea surface, and has been a popular approach in dynamic soaring modeling. However, recent studies have argued that the real sea surface is not flat, and wind separations in ocean waves may occur more often than expected (44). To describe wind-separation-like wind profiles, a sigmoidal model has been proposed (19, 45). We also employed the sigmoidal wind model with a minor change, represented as

[Sigmoidal wind gradient model]

$$W_{\mathrm{Sigmoid}}(z) = \frac{W_{\max}}{1 + \mathrm{e}^{-\frac{z-h_{\mathrm{W}}}{\delta}}} \quad [13].$$

h_w determines the height of wind separation, as shown in Fig. 3. In this study, we set h_w to 1, 3, and 5. δ is the thickness parameter. The wind speed changes with height ($|z - h_w| \lesssim 3\delta$ m). In a previous study, the wind shear thickness was speculated as approximately 1.5–7 m. Here, we set δ to 3/6 with a steep wind change, and 7/6 with a gentler change (Fig. 3).

Formulation to numerical optimization

The numerical computation of dynamic soaring performance and minimum wind speed boiled down to the restricted optimization problem. That is, a mathematical problem to find the values of (i) a certain variable ***Y*** that maximizes (ii) an objective function *f*(***Y***), satisfying (iii)

equalities $\boldsymbol{h}(\boldsymbol{Y}) = 0$ and (iv) inequalities $\boldsymbol{g}(\boldsymbol{Y}) \leqq 0$. In the following, we describe the variables, object functions, equalities, and inequalities for dynamic soaring.

(i) Variables

The dynamics of dynamic soaring animals are described by the 3D position (x(t), y(t), z(t)), pitch angle $\gamma(t)$, yaw angle $\psi(t)$, airspeed $V(t)$, bank angle $\phi(t)$, lift coefficient C_L, and the period of one dynamic soaring cycle τ. Among these variables, 3D position, pitch, yaw, bank, and airspeed are functions of time t ($0 \leq t \leq \tau$). Optimization problems that include functions as variables are difficult to be directly solved. Therefore, we employed a collocation approach (19, 46). The collocation approach discretizes the variables in time, such as X(t) ($0 \leq t \leq \tau$) to variables $X_i = X((i\text{-}1)N/\tau)$ (i = 1, N), and converts the EOM to the equalities between those discretized variables. Hereafter, we use $X_{1:N} = \{X_1, X_2, \ldots, X_N\}$. In this study, we set the number of discretization points to N = 51 in order to perform computations with reasonable accuracy within a reasonable amount of time. Accordingly, the variables of this optimization problem are position $x_{1:N}, y_{1:N}, z_{1:N}$, pitch angle $\gamma_{1:N}$, yaw angle $\psi_{1:N}$, airspeed $V_{1:N}$, bank angle $\phi_{1:N}$, lift coefficient C_L, and a period of one soaring cycle τ. In addition, when computing the minimum wind speed required for sustainable dynamic soaring, W_{10} (log model) or W_{max} (sigmoid model) were also treated as variables. Hence, the total number of variables were 7 × 51 + 2 (+1) = 359 (or 360).

(ii) Object function

First, we computed (1) the minimum wind speed required for sustainable dynamic soaring for each wind gradient model. As the objective function to minimize, we set W_{10} for the logarithmic model and W_{max} for the sigmoidal model. Then, we computed (2) the maximum speed averaged over one dynamic soaring cycle by maximizing the object function to $\sqrt{x_N^2 + y_N^2}/\tau$. Finally, we computed (3) the maximum upwind speed averaged over one dynamic soaring cycle by maximizing the object function y_N/τ. With respect to the maximum speed and maximum windward speed, we computed these values for different wind speeds, that is, from the minimum required wind speed of the species to the highest minimum required wind speed among the examined species (i.e., *Quetzalcoatlus*) +2 m/s. In this wind speed range, the maximum speed reached an unrealistically high value and/or the optimization calculation did not converge for some species. Thus, we stopped the computation of the maximum speed at the wind speed where the maximum speed exceeded 40 m/s (144 km/h).

(iii) Equalities

The first equalities to be fulfilled for dynamic soaring animals are given in Eq. 3–8. The collocation approach converts the EOM into the equalities between the variables listed in the above section. As the number of original EOM was six and the number of discretization was 51, the EOM were converted into 6 × 51 = 306 equalities (see (19, 46) for the specific representations of these equalities).

The second type of equalities to be fulfilled were periodic boundary conditions of dynamic soaring: at the beginning and end of one dynamic soaring cycle, the state of the animal (i.e., pitch, yaw, airspeed, bank, height) is the same, represented as

$$z_1 = z_N, \gamma_1 = \gamma_N, \psi_1 = \psi_N, \phi_1 = \phi_N, V_1 = V_N \qquad [14].$$

(iv) Inequalities

First, we assumed that there was a maximum limit of physical load on the animal. This is because dynamic soaring entails dynamic maneuvering, which results in a corresponding acceleration. We employed the approach of a previous study (18) that restricted the load factor (L/mg) to less than 3,

$$\frac{L}{mg} \leq 3 \qquad [15].$$

The second inequality was an important modification of the previous models. The height of the animal's wingtip (z_{wing}) was calculated as above the sea surface and was represented as

$$z_{\text{wing}} = z - \frac{b}{2} \sin\phi \cos\gamma \geq 0 \qquad [16].$$

Previous studies discarded the existence of the sea surface (19) or restricted birds to only flying higher than a given height (1.5 m) from the sea surface (18). However, the height a bird can fly depends on the wing length and the bank angle (e.g., with a shorter wing length and a lower bank angle, a bird can fly at a lower height). When dynamic soaring birds fly, they adjust their wingtips close to, but avoid touching, the sea surface (Fig. 3D). Dynamic soaring birds can

exploit more flight energy when they pass through stronger wind speed differences. As the wind speed difference is strong close to the sea surface, how close to the sea surface a bird can fly is crucial for dynamic soaring birds. Accordingly, long wings may restrict the minimum height at which the bird can fly and disturb efficient dynamic soaring. Hence, considering the effect of wings is crucial for evaluating dynamic soaring performances.

Third, we also assumed that the height of the animal was higher than 0.5 m, that is,

$$z \geq 0.5 \qquad [17].$$

The optimization problem described here is a restricted non-linear optimization problem. We used the SQP method to solve the problem with the "fmincon" function in MATLAB® Ver R2019a.

<u>Quantification of the thermal soaring performance and the required minimum upward wind speed</u>

For the computation of glide polars and circling envelopes, we followed the same procedure as the *Flight* software developed for evaluating bird flight performance, as described in (16). In the following, we outline the procedure and parameters employed in this study.

First, before computing the glide polars, we determined how gliding animals adjust their wing area with respect to their airspeed. We assumed that the wingspan decreases as a linear function of speed, based on observations in real birds (47). We employed *Flight*'s default setting, which assumes that wingspan, wing area, and thus aspect ratio linearly decrease with factor $\beta = (B_{\mathrm{stop}} - V/V_S)/(B_{\mathrm{stop}} - 1)$; i.e., we replaced b, S_{W}, and R_{a} with βb, βS_{W}, and βR_{a}, respectively. In this equation, V_S is the stall speed, the airspeed of the animal at the highest lift coefficient (i.e., $V_s = \sqrt{(2mg)/(\rho S_{\mathrm{W}} C_{\mathrm{Lmax}})}$); and B_{stop} is a constant that determines the degree of wing reduction. For birds, we set B_{stop} to 5, the default value in *Flight*. For pterosaurs, we set B_{stop} to 6, following a previous study (14). Then, the glide polars were derived from the EOM, setting bank angle to 0, assuming that the pitch angle was small enough ($\gamma \ll 1$) and considering the gliding animal was at kinematical equilibrium ($mg = \sqrt{L^2 + D^2} \simeq L,\ \sin\gamma = D/L \simeq L/mg$). Sinking speed was represented as a function of airspeed V (16),

$$V_{\mathrm{Sink}} = \frac{\rho}{2}\left(\frac{S_{\mathrm{W}}}{mg}\right)\left(C_{\mathrm{Dpro}}\beta + 0.01\right)V^3 + \left(\frac{mg}{S_{\mathrm{W}}}\right)\left(\frac{2k}{\rho R_{\mathrm{a}}\beta^2\pi}\right)\frac{1}{V} \qquad [18].$$

This relation gives a glide polar. Note that we used eq. 11 (C_{Dpar} S_B = 0.01Sw; in this equation, S_W was not replaced with βS_W) to derive the above equation. The horizontal speed is $\sqrt{V^2 - V_{\mathrm{Sink}}^2}$. Thus, the maximum glide ratio is the maximum value of $\sqrt{V^2 - V_{\mathrm{Sink}}^2}/V_{\mathrm{Sink}}$.

The circling envelope is given with the radius of the circle (r), and the sinking speed in a circling glide ($V_{\mathrm{Sink,Circle}}$) is represented by the bank angle (ϕ),

$$r = \frac{2m}{C_{\mathrm{L}}^{*} S_{\mathrm{W}} \rho \sin\phi} \qquad [19]$$

and

$$V_{\mathrm{Sink,Circle}} = \frac{V_{\mathrm{Sink,min}}}{(\cos\phi)^{3/2}} \qquad [20],$$

where C_L^* and $V_{\mathrm{Sink,min}}$ are the lift coefficient and the sinking speed at the minimum sinking speed of the glide polar, respectively (16).

Acknowledgments: The authors thank Chihiro Kinoshita for illustrating Fig. 1. We thank Fujiwara Shin-ichi for reading the draft of this paper and for providing valuable comments. This study was financially supported by Grants-in-Aid for Scientific Research from the Japan Society for the Promotion of Science (16H06541, 16H01769), and JST CREST Grant Number JPMJCR1685, Japan.

Notes: The authors declare no competing interest.

References

1. Ksepka DT (2014) Flight performance of the largest volant bird. *Proc Natl Acad Sci* 111(29):10624–10629.
2. Campbell Jr KE, Tonni EP (1981) Preliminary observations on the paleobiology and evolution of teratorns (Aves: Teratornithidae). *J Vertebr Paleontol* 1(3–4):265–272.
3. Campbell Jr KE, Tonni EP (1983) Size and locomotion in teratorns (Aves: Teratornithidae). *Auk* 100(2):390–403.

4. Chatterjee S, Templin RJ, Campbell Jr KE (2007) The aerodynamics of Argentavis, the world's largest flying bird from the Miocene of Argentina. *Proc Natl Acad Sci* 104(30):12398–12403.
5. Witton MP (2008) A new approach to determining pterosaur body mass and its implications for pterosaur flight. *Zitteliana* B28:143–158.
6. Frey E, Martill DM (1996) A reappraisal of Arambourgiania (Pterosauria, Pterodactyloidea): one of the world's largest flying animals. *Neues Jahrb für Geol und Paläontologie–Abhandlungen* 199:221–247.
7. Buffetaut E, Grigorescu D, Csiki Z (2003) Giant azhdarchid pterosaurs from the terminal Cretaceous of Transylvania (western Romania). *Geol Soc London, Spec Publ* 217(1):91–104.
8. Hone DWE, Habib MB, Therrien F (2019) Cryodrakon boreas, gen. et sp. nov., a Late Cretaceous Canadian Azhdarchid Pterosaur. *J Vertebr Paleontol* 39(3):e1649681.
9. Vremir M, Dyke G, Csiki-Sava Z, Grigorescu D, Buffetaut E (2018) Partial mandible of a giant pterosaur from the uppermost Cretaceous (Maastrichtian) of the Haţeg Basin, Romania. *Lethaia* 51(4):493–503.
10. Sato K, et al. (2009) Scaling of soaring seabirds and implications for flight abilities of giant pterosaurs. *PLoS One* 4(4):e5400.
11. Habib MB (2008) Comparative evidence for quadrupedal launch in pterosaurs. *Zitteliana* B28:159–166.
12. Cannell AER (2020) Too big to fly? An engineering evaluation of the fossil biology of the giant birds of the Miocene in relation to their flight limitations, constraining the minimum air pressure at about 1.3 bar. *Anim Biol* 1(aop):1–20.
13. Chatterjee S, Templin RJ (2004) *Posture, locomotion, and paleoecology of pterosaurs* (Geological Society of America).
14. Witton MP, Habib MB (2010) On the size and flight diversity of giant pterosaurs, the use of birds as pterosaur analogues and comments on pterosaur flightlessness. *PLoS One* 5(11):e13982.
15. Palmer C (2011) Flight in slow motion: aerodynamics of the pterosaur wing. *Proc R Soc B Biol Sci* 278(1713):1881–1885.
16. Pennycuick CJ (2008) *Modelling the flying bird* (Elsevier).

17. Pennycuick CJ (1983) Thermal soaring compared in three dissimilar tropical bird species, Fregata magnificens, Pelecanus occidentals and Coragyps atratus. *J Exp Biol* 102(1):307–325.
18. Sachs G (2005) Minimum shear wind strength required for dynamic soaring of albatrosses. *Ibis*147(1):1–10.
19. Bousquet GD, Triantafyllou MS, Slotine J-JE (2017) Optimal dynamic soaring consists of successive shallow arcs. *J R Soc Interface* 14(135):20170496.
20. Palmer C, Dyke GJ (2010) Biomechanics of the unique pterosaur pteroid. *Proc R Soc B Biol Sci* 277(1684):1121–1127.
21. Henderson DM (2010) Pterosaur body mass estimates from three-dimensional mathematical slicing. *J Vertebr Paleontol* 30(3):768–785.
22. Bramwell CD, Whitfield GR (1974) Biomechanics of pteranodon. *Philos Trans R Soc London B, Biol Sci* 267(890):503–581.
23. Brower JC (1983) The aerodynamics of Pteranodon and Nyctosaurus, two large pterosaurs from the Upper Cretaceous of Kansas. *J Vertebr Paleontol* 3(2):84–124.
24. Venditti C, Baker J, Benton MJ, Meade A, Humphries S (2020) 150 million years of sustained increase in pterosaur flight efficiency. *Nature*. doi:10.1038/s41586-020-2858-8.
25. Wilkinson MT, Unwin DM, Ellington CP (2006) High lift function of the pteroid bone and forewing of pterosaurs. *Proc R Soc B Biol Sci* 273(1582):119–126.
26. Taylor GK, Thomas ALR (2014) *Evolutionary biomechanics: selection, phylogeny, and constraint* (Oxford Series in Ecology and Evolution).
27. Wilkinson MT (2008) Three-dimensional geometry of a pterosaur wing skeleton, and its implications for aerial and terrestrial locomotion. *Zool J Linn Soc* 154(1):27–69.
28. Bennett SC (2003) Morphological evolution of the pectoral girdle of pterosaurs: myology and function. *Geol Soc London, Spec Publ* 217(1):191–215.
29. Norberg UM, Rayner JMV (1987) Ecological morphology and flight in bats (Mammalia; Chiroptera): wing adaptations, flight performance, foraging strategy and echolocation. *Philos Trans R Soc London B, Biol Sci* 316(1179):335–427.

30. Norberg UM (2012) *Vertebrate flight: mechanics, physiology, morphology, ecology and evolution* (Springer Science & Business Media).
31. Witton MP, Naish D (2008) A reappraisal of azhdarchid pterosaur functional morphology and paleoecology. *PLoS One* 3(5):e2271.
32. Witton MP, Naish D (2013) Azhdarchid pterosaurs: water-trawling pelican mimics or "terrestrial stalkers"? *Acta Palaeontol Pol* 60(3):651-660.
33. Sachs G, Weimerskirch H (2018) Flight of frigatebirds inside clouds-energy gain, stability and control. *J Theor Biol* 448:9-16.
34. Swaminathan B, Mohan R (2018) On The Stability of Dynamic Soaring Orbits of UAVs. *2018 Atmospheric Flight Mechanics Conference*, p 2832.
35. Sachs G, Traugott J, Nesterova AP, Bonadonna F (2013) Experimental verification of dynamic soaring in albatrosses. *J Exp Biol* 216(22):4222-4232.
36. Harel R, Horvitz N, Nathan R (2016) Adult vultures outperform juveniles in challenging thermal soaring conditions. *Sci Rep* 6:1-8.
37. Sherub S, Bohrer G, Wikelski M, Weinzierl R (2016) Behavioural adaptations to flight into thin air. *Biol Lett* 12(10):20160432.
38. Williams HJ, et al. (2018) Vultures respond to challenges of near-ground thermal soaring by varying bank angle. *J Exp Biol* 221(23).
39. Shimatani IK, Yoda K, Katsumata N, Sato K (2012) Toward the quantification of a conceptual framework for movement ecology using circular statistical modeling. *PLoS One* 7(11):e50309.
40. Treep J, et al. (2015) Using high resolution GPS tracking data of bird flight for meteorological observations. *Bull Am Meteorol Soc* 97:951-961.
41. Weinzierl R, et al. (2016) Wind estimation based on thermal soaring of birds. *Ecol Evol* 6(24):8706-8718.
42. Yonehara Y, et al. (2016) Flight paths of seabirds soaring over the ocean surface enable measurement of fine-scale wind speed and direction. *Proc Natl Acad Sci* 113:9039-9044.
43. Goto Y, Yoda K, Sato K (2017) Asymmetry hidden in birds' tracks reveals wind, heading, and orientation ability over the ocean. *Sci Adv* 3(9):e1700097.
44. Buckley MP, Veron F (2016) Structure of the airflow above surface waves. *J Phys Oceanogr* 46(5):1377-1397.

45. Bird JJ, Langelaan JW, Montella C, Spletzer J, Grenestedt J (2014) Closing the loop in dynamic soaring. *AIAA Guidance, Navigation, and Control Conference*, p 263.
46. Zhao YJ (2004) Optimal patterns of glider dynamic soaring. *Optim Control Appl methods* 25(2):67–89.
47. Rosén M, Hedenstrom A (2001) Gliding flight in a jackdaw: a wind tunnel study. *J Exp Biol* 204(6):1153–1166.
48. Shaffer SA, Weimerskirch H, Costa DP (2001) Functional significance of sexual dimorphism in wandering albatrosses, Diomedea exulans. *Funct Ecol* 15(2):203–210.
49. Phillips RA, Silk JRD, Phalan B, Catry P, Croxall JP (2004) Seasonal sexual segregation in two Thalassarche albatross species: competitive exclusion, reproductive role specialization or foraging niche divergence? *Proc R Soc London Ser B Biol Sci* 271(1545):1283–1291.
50. Pennycuick CJ (1987) Flight of auks (Alcidae) and other northern seabirds compared with southern Procellariiformes: ornithodolite observations. *J Exp Biol* 128(1):335–347.